Nocturnal boundary layer turbulence regimes analysis during the BLLAST campaign

Jesús Yus-Díez[1,5], Mireia Udina[1], Maria Rosa Soler[1], Marie Lothon[2], Erik Nilsson[3], Joan Bech[1], and Jielun Sun[4]

[1]Departament de Física Aplicada - Meteorologia, Universitat de Barcelona, C/Martí i Franquès, 1., 08028, Barcelona, Spain
[2]Laboratoire d'Aérologie, University of Toulouse, CNRS, France
[3]Department of Earth Sciences, Uppsala University, Uppsala, Sweden
[4]NorthWest Research Associates, Boulder, Colorado, USA
[5]Institute of Environmental Assessment and Water Research (IDAEA-CSIC), C/Jordi Girona 18-26, 08034, Barcelona, Spain

**Correspondence:** Jesús Yus-Díez (jesus.yus@idaea.csic.es), Mireia Udina (mudina@meteo.ub.edu)

Abstract. A night-time turbulence regime classification, the so-called HOckey-Stick Transition (HOST) theory, proposed by Sun et al. (J Atmos Sci 69(1):338-351, 2012) from the Cooperative Atmosphere-Surface Exchange Study 1999 (CASES-99) is explored using data from the Boundary-Layer Late Afternoon and Sunset Turbulence (BLLAST) field campaign which took place during the summer 2011 in the central French Pyrenean foothills.

Results show that the HOST turbulence relationships for the BLLAST field campaign data are strongly dependent on both the meteorological and orographic features. The HOST pattern only appears for nights when a stably stratified boundary layer can be developed, corresponding to fair weather and clear sky nights, when the flow is generated by the nearby orography, from the south and south-east directions. Those flows strongly influenced by the orography may generate intermittent or enhanced turbulence. When considering the whole nocturnal dataset for these flow directions, several enhanced turbulence points are found to be associated with sudden wind speed and directional shear transitions. In contrast, flows from other directions do not reproduce the HOST relationships and the turbulence relationship is almost linear, independent of vertical temperature gradients, corresponding to flows driven by synoptic scales. In addition we identify examples of gravity waves and top-down turbulent events that lead to transitions between the turbulence regimes.

Copyright statement. TEXT

1 Introduction

With the aim to investigate and categorise turbulence patterns generated by wind shear in the atmospheric stable boundary layer (SBL), Sun et al. (2012) analysed a month-long dataset collected in Kansas from the Cooperative Atmosphere-Surface Exchange Study in October 1999 (CASES-99) (Poulos et al., 2002). They found that, depending on the relationship between the turbulence intensity of the flow and the wind velocity, turbulent mixing from the surface to the last level of measurement
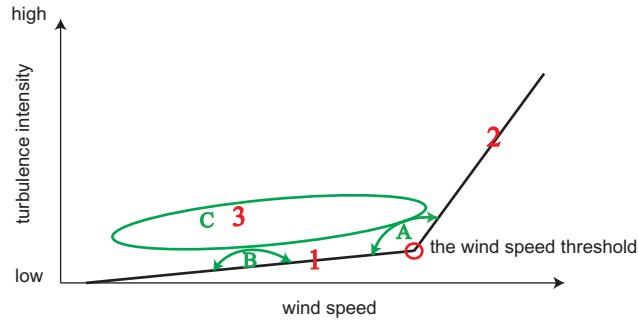
Figure 1. Schematic representation of the HOckey-STick (HOST) theory with the three turbulence regimes (regime 1, 2 and 3) and the three turbulence intermittency categories (category A, category B and category C). Reproduced from Figure 2 of Sun et al. (2012) ©American Meteorological Society. Used with permission.

(55m) can be categorised in three regimes (Fig. 1). A regime 1 occurring when the wind speed (V) is less than a threshold value (V_T), characterised by low turbulence intensity increasing slightly with the velocity. This is the weak turbulence regime, which is generated by local shear and modulated by the vertical temperature gradients of the SBL. Eddies generated by local shear, $\delta V/\delta z$, do not interact with the ground as their length scale is smaller than the observation height z, $\delta z < z$ (Sun et al., 2012). When $V > V_T$ regime 2 occurs and turbulence is mainly driven by the bulk shear, therefore increasing strongly and nearly linearly with V. The close relationship between turbulence intensity and mean wind speed suggests that near the ground, turbulence under moderate winds responds to the bulk shear $V(z)/z$ (Sun et al., 2012, 2016). The eddies dominating this stronger turbulence regime have a larger scale of z, thus leading to a well mixed layer below this height and producing a near-neutral stratification. The value of the wind speed threshold at which the shear changes from local to bulk increases with height approximately logarithmically (Sun et al., 2012; Bonin et al., 2015). In addition to these two turbulent regimes generated by the local or the bulk shear, moderate turbulence can be often generated for relative low values of V and large stability conditions above the observation level by different coherent structures, for instance: Kelvin- Helmholtz instabilities (Newsom and Banta, 2003), gravity waves (Sun et al., 2004; Udina et al., 2013), and density currents (Sun et al., 2002; Viana et al., 2010; Soler et al., 2014) which can generate turbulence, that is transported downward, toward observation levels where the wind speed is lower than the threshold value. This top-down turbulent regime is defined as regime 3, which also includes turbulence enhanced by wind shear associated with topographical features leading to flow accelerations, directional wind shear and sub-meso motions (Mahrt et al., 2013). All these intermittent turbulent events have in common the non-stationarity of the flow.

The schematic representation of the transition between the weak and the strong turbulence regimes resembles a Hockey-Stick (Fig. 1), this is why this theory is named HOckey-Stick Transition (HOST). It can be explained in terms of total turbulence energy (TTE) defined as the sum of the turbulent kinetic energy (TKE) and the turbulent potential energy (TPE), also called available potential energy (Zilitinkevich et al., 2007). As shown in Sun et al. (2016), if the vertical variation of TTE is small, the turbulence shear production controls the variation of TTE. When $V < V_T$ the vertical transport of cold air is confined near the

surface, the stable stratification of the flow increases. Therefore more turbulence energy is used to increase the TPE (Lin and Pao, 1979), and TKE does not increase significantly with increasing $V(z)$. This situation corresponds to regime 1. However, if $V > V_T$ the stable stratification is considerably reduced, leading to a near-neutral regime. As a consequence, shear generates TKE as the TTE is not consumed to increase TPE, this situation corresponds to regime 2.

5   The HOST theory represents a new approach for the turbulence parameterisation in the surface layer, as the Monin Obukhov Similarity Theory (MOST) may be limited, because the bulk formulae are applicable only within a near thin surface layer (Sun et al., 2012, 2016). The theory has been previously studied for other campaigns and sites in relatively flat terrain areas. Mahrt et al. (2013) studied the turbulence behaviour in three sites with different surface roughness, showing that the wind speed threshold decreases with increasing roughness length; Andreae et al. (2015) explored the three turbulence regimes and
10   characterised the nocturnal boundary layer using data from The Amazon Tall Tower Observatory (ATTO); Bonin et al. (2015) used the HOST via remote sensing in the Southern Great Plains and Acevedo et al. (2016) studied the HOST theory via the contrasting structures of the stable and neutral states of the boundary layer over snow-covered surfaces. The theory has also been investigated through large eddy simulation (LES) models (Udina et al., 2016), revealing the LES difficulties to reproduce regime 1.

15   As the HOST was originally derived from measurements taken in a relatively flat area, where the CASES-99 field campaign was held (Sun et al., 2012), the aim of this study is to explore the validity of the HOST theory in a complex terrain area, for flows that are influenced by the nearby orography. This study considers nocturnal boundary layers with special emphasis in the very stable boundary layer. The data analysed herein is from the Boundary Layer Late Afternoon and Sunset Turbulence (BLLAST) campaign (Lothon et al., 2014), which took place during early summer of 2011 in France, in the "Plateau de
20   Lannemezan", north of the central French Pyrenean foothills.

The structure of the paper is as follows. The site, the in situ observations of near surface turbulence obtained from the array of instruments and the data processing method applied are described in Sect. 2. The wind flow and wind regimes affecting the site during the BLLAST field experiment are analysed in Sect. 3. The categorisation of the turbulence regimes patterns for the BLLAST field campaign is investigated in sections 4 and 5, while the transition between regimes is illustrated in Sect. 6 using
25   selected examples. A summary and the main conclusions are given in Sect. 7.

2   Site, observations and data processing

Data used in this study comes from the BLLAST field campaign conducted in early summer, from 14 June to 8 July 2011 in France around the Centre for Atmospheric Research (CRA, *Centre de Recherches Atmosphériques*) (Lothon et al., 2014). The site (site 1 in Fig. 2a) is located in the "Plateau de Lannemezan", which is a plateau over the Garonne basin at about 600 m
30   above sea level (a.s.l.). The plateau is about 11 km north from the base of the first range of the Pyrenees with peaks of around 1500-2000 m a.s.l. and about 40 km away of the highest peaks of the Pyrenees mountain range.
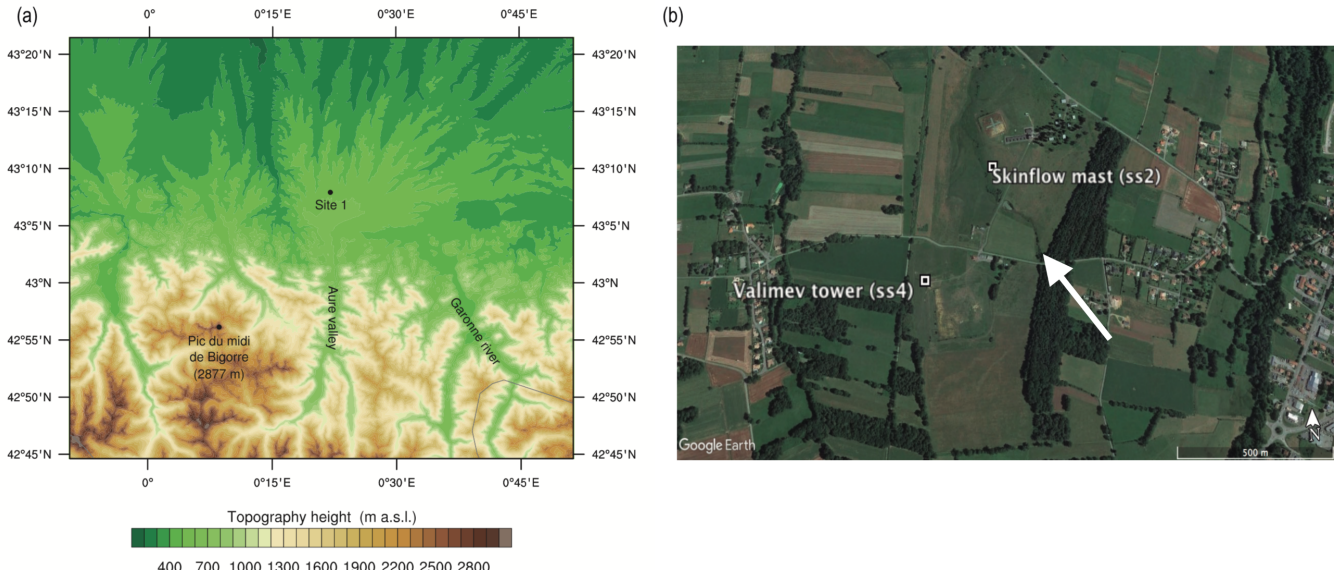
Figure 2. Location of the "Plateau de Lannemezan" and the surrounding area with: (a) a topographical map of the surroundings of site 1 where the BLLAST field campaign took place showing terrain elevation of the area, with the Pyrenees mountain range at its south and the location of the Aure valley and the Garonne river; (b) satellite view of site 1 showing the location of the Skinflow mast at surface-site 2 (ss2), the Valimev tower at surface-site 4 (ss4) and a small gully south-east of the Skinflow mast (white arrow).

The site is influenced by both the steep orography surrounding it at the south-west (Pic du midi de Bigorre) as well as the exit of the Aure valley (Aura in local occitan language) at the south at around 11 km. The Garonne upper-valley is at the east-southeast (Fig. 2a).

The main objective of the BLLAST field campaign was to improve the knowledge of the afternoon and evening transition
5   in the Boundary Layer (BL) (Lothon et al., 2014). To achieve this, a dense array of instrumentation was deployed over the area, although only some of them are employed herein (Table 1). We focus the analysis on the data from the 10 m mast of the surface-site 2 (ss2), called Skinflow mast, and the 60 m tower placed at the surface-site 4 (ss4), called Valimev tower (Fig. 2b). From the Skinflow mast we use data from the sensors located at 2.23 m, 3.23 m, 5.27 m and 8.22 m (named hereafter z_{2m}, z_{3m}, z_{5m} and z_{8m}, respectively), although the z_{2m} level is omitted when the values are very close to those of z_{3m}. From the
10   Valimev tower we use data from the sensors located at 29.4 m, 45.8 m and 61.4 m (named hereafter z_{30m}, z_{45m} and z_{60m}, respectively), see Table 1.

Since the analysis is restricted to the night-time, we only consider data measured from 1942 UTC to 0420 UTC (Lothon et al., 2014; Blay-Carreras et al., 2014) which is representative of the sunrise and sunset time during this period and at this area. An alternative method to select the study periods would be to consider the time when sensible heat flux changes its sign
15   instead of the sunset and sunrise but the first approach was followed for consistency with previous studies.

Table 1. Skinflow mast and Valimev tower sonic measurements from the BLLAST field campaign used in this study.

Level name	Height [m]	Measured variables	Sensors	Data period
z_{2m}	2.23			
z_{3m}	3.23		Campbell Thermocouple E-Type FW05	19 June 2011 - 8 July 2011
z_{5m}	5.27	T [°C], (u,v,w) [m s^{-1}]	Campbell Csat3 3D sonic anemometer	
z_{8m}	8.22			
z_{30m}	29.4		Campbell Csat3 3D sonic anemometer	14 June 2011 - 8 July 2011
z_{45m}	45.8		Gill master pro 3D sonic anemometer, wind vane	
z_{60m}	61.4		Campbell Csat3 3D sonic anemometer	15 June 2011 - 8 July 2011

Two datasets with different sampling frequency were used from Skinflow mast levels between z_{2m} and z_{8m}: thermocouples (1 Hz) and sonic anemometers (10 Hz) (Table 1).The timespan of available measurements for the Skinflow mast levels starts on 19 June 2011 and finishes on 8 July 2011. For the statistical study of the behavior of the turbulence strength relationship with the wind speed we set a temporal average of 5 min as done in Sun (2011); Sun et al. (2012); Mahrt (2014). We used this temporal

5 average because reducing the averaging period, or using other methods as multi-resolution decomposition or wavelet, migth potentially eliminate the contribution of non-turbulent mesoscale motions to the calculated turbulence quantities (Terradellas et al., 2005; Udina et al., 2013; Ferreres et al., 2013; Soler et al., 2014). However, to obtain a broad picture of the patterns, a constant averaging time of 5 min. has seemed sufficient. In addition, as Mahrt (2017) stated, in very stable conditions, variation of turbulent fluxes on time-scales of a few minutes to tens of minutes are often associated with short periods of

10 near-calm conditions where the turbulent fluxes are particularly small, and as a result its values are not very dependent on the averaging time. The high frequency signal of the turbulence is used to calculate average statistics to show a broad picture of the patterns. Whereas when the aim is to show with more detail the temporal evolution of the turbulent variables, a small temporal average set with averages ranging between 10 s and 1 min is obtained. This high-frequency procedure aims to account for the turbulence intermittency within and between the different turbulent regimes defined in the HOST theory. In the atmospheric

15 boundary layer (ABL), intermittency is basically found on the stable boundary layer (SBL) over land at night, especially under conditions of large static stability and strong vertical wind shear, when turbulence is sporadic, characterized by bursts or episodes with periods of relatively weak or un-measurable small fluctuations. In this paper we use the term "intermittency", to describe specifically a temporal variation of turbulence intensity or turbulence strength, represented by the V_{TKE} value calculated at a fixed location, as Sun et al., 2012. Reasons for increased turbulence are diverse and may include the intrusion

20 of coherent structures such as gravity waves, density currents (Terradellas et al., 2005; Udina et al., 2013; Ferreres et al., 2013; Soler et al., 2014) and low-level jets (LLJs) (Mahrt, 1999; Newsom and Banta, 2003; Cuxart and Jiménez, 2007).

From the Valimev 60 m tower we have used the measurements from the sonic anemometers located at the z_{30m}, z_{45m} and z_{60m} levels, as shown in Table 1. The dataset for this tower starts on 14 June 2011 for the z_{30m} and z_{45m} levels, and slightly

later for z_{60m}, between 1000-1100 UTC of 15 June 2011, and finishes on 8 July 2011 for the three levels. The same data processing as to the Skinflow mast levels measurements is applied to the Valimev levels, using temporal averages of 5 min and averages ranging between 10 s and 1 min as well.

We follow the corrections and filters indicated in Said et al. (2011a, b) and De Coster et al. (2011) report, where the post-processing applied to the BLLAST data is explained in detail (e.g. applying a planar-fit rotation to the wind direction dataset). Additionally, sonic measurements were not considered when anomalous V_{TKE} values were observed during rainfall periods.

We calculate several parameters in order to study the turbulence regimes relationships: the wind speed, V:

$$V = \sqrt{u^2 + v^2} \tag{1}$$

where u and v are the horizontal wind components; the turbulence intensity or turbulence strength, V_{TKE}:

$$V_{TKE} = \sqrt{\frac{1}{2}(\sigma_V^2 + \sigma_w^2)} \tag{2}$$

where σ represents the standard deviation of the wind components, and $\sigma_V^2 = \sigma_u^2 + \sigma_v^2$; the potential virtual temperature:

$$\theta_v = T_v + \Gamma_d z \tag{3}$$

where T_v is the virtual temperature at each height z and Γ_d is the dry adiabatic lapse rate; and the skewness of the vertical velocity fluctuations (Wyngaard, 2010):

$$S_w = \frac{\overline{w'(z)^3}}{\left(\overline{w'(z)^2}\right)^{3/2}} \tag{4}$$

which gives us information about the vertical transport (upward or downward) of the vertical velocity variance.

Furthermore, when the relationship V_{TKE} vs V is graphically analysed we use the bin-average technique where we group the data into wind speed bins of 0.4 m s^{-1} starting at a wind speed of 0.1 m s^{-1}. For each of those bins it is displayed the median value with the corresponding error bars. These error bars represent the first and third quartiles instead of the actual standard deviation as a consequence of the skewed distribution of the turbulence points for each wind speed bin. This bin-averaged technique is also employed for the box plot analysis. In addition, we have made an exhaustive analysis in order not to consider the measurements collected under strong precipitation events, where the sonic anemometers do not work properly.

## 3 Flow characterisation during the BLLAST field campaign

The objective of the paper is to study how the HOST theory behaves in the complex terrain environment for the BLLAST field experiment in the nocturnal boundary layer. In the area, during night-time when thermally-driven flows can be developed, a katabatic flow going down from the mountain to the plain is established, through valley and downslope winds (Román-Cascón et al., 2015; Román-Cascón et al., 2019). Since the HOST theory proposed by Sun et al. (2012, 2016) during the CASES-99 campaign corresponds to nights with clear skies and intense radiative cooling allowing the development of local and mesoscale

Table 2. Night-time data, between 1942 and 0420 UTC, of the Skinflow mast and Valimev tower levels considered as IOPs nights. The temporal series starts the 14 of June for the first two levels with sonic anemometers of the Valimev tower, and the 15 of June for z_{60m}; for the Skinflow data, the measurements began the 19 of June.

nIOP	Corresponding night-time IOP	Date (dd/mm)	Levels
nIOP00	IOP00-IOP01	14/06-15/06	z_{30m}, z_{45m}
nIOP01	IOP02-IOP03	19/06-20/06	$z_{30m} - z_{60m}$
nIOP02	IOP03	20/06 (1942-2359 UTC)	$z_{3m} - z_{60m}$
nIOP03	IOP04-IOP05	24/06-25/06	$z_{3m} - z_{60m}$
nIOP04	IOP05-IOP06	25/06-26/06	$z_{3m} - z_{60m}$
nIOP05	IOP06-IOP07	26/06-27/06	$z_{3m} - z_{60m}$
nIOP06	IOP07	27/06 (1942-2100 UTC)	$z_{3m} - z_{60m}$
nIOP07	IOP08-IOP09	30/06-01/07	$z_{3m} - z_{60m}$
nIOP08	IOP09-IOP10	01/07-02/07	$z_{3m} - z_{60m}$
nIOP09	IOP10 - 03/07	02/07-03/07	$z_{3m} - z_{60m}$
nIOP10	IOP11	05/07 (0000 - 0420 UTC)	$z_{3m} - z_{60m}$

winds, we first select the nights that meet these conditions during the BLLAST campaign. This is done similarly as Lothon et al. (2014) selected the intensive observation periods (IOPs) in BLLAST, focused on the diurnal and the late-afternoon transition boundary layer analysis. Instead, we consider as a IOP night, hereafter nIOP, the period between 1942 UTC of that IOP day and 0420 UTC of the following day (Blay-Carreras et al., 2014). That is, the evening, night and early morning following an

5   IOP day, excluding any nocturnal period strongly influenced by larger scale phenomena, such as a synoptic frontal system or mesoscale convective systems. In the case when the night-time period prior to the IOP shows the typical nocturnal flow cycle, we do consider the early morning of the corresponding IOP, i.e. from 0000 to 0420 UTC. Following these criteria, table 2 shows the nocturnal periods considered as nIOPs.

    To characterise the wind flow regimes on the Plateau de Lannemezan for the nIOPs, the first step is to calculate the wind

10   roses for each level of measurement, both for the Skinflow mast and the Valimev tower. Fig. 3 shows that 25 % of the flows at the lower levels, $z_{3m} - z_{8m}$, come from the south-east quadrant, which correspond to shallow drainage flows, formed after sunset due to local and very small slopes located in the foothills of the Pyrenees (Román-Cascón et al., 2015)). These authors tested that up to 4 days of the BLLAST campaign presents SDFs after the near calm period of the afternoon, exhibiting a wind maxima, around $1.5 - 2 \, \mathrm{m \, s^{-1}}$ close to the surface, in the first 5 m a.g.l.. At higher levels, $z_{30m} - z_{60m}$, wind roses show a large

15   fraction of winds coming from the south-east quadrant (35 % of the data), which are associated with the larger scale mountain plain flows (MPFs). In this case the location of the maximum wind is higher, at 80 m as state Román-Cascón et al. (2015), or between 50 and 200 m corresponding to the Aura valley exit flow (Jiménez et al., 2019). To document the SDFs and the MPFs, we present an example shown in Román-Cascón et al. (2015) between noon of the 2nd of July and the morning of the 3rd July 2011, including nIOP09. The predominant direction during the central part of the day-time is from the north corresponding to
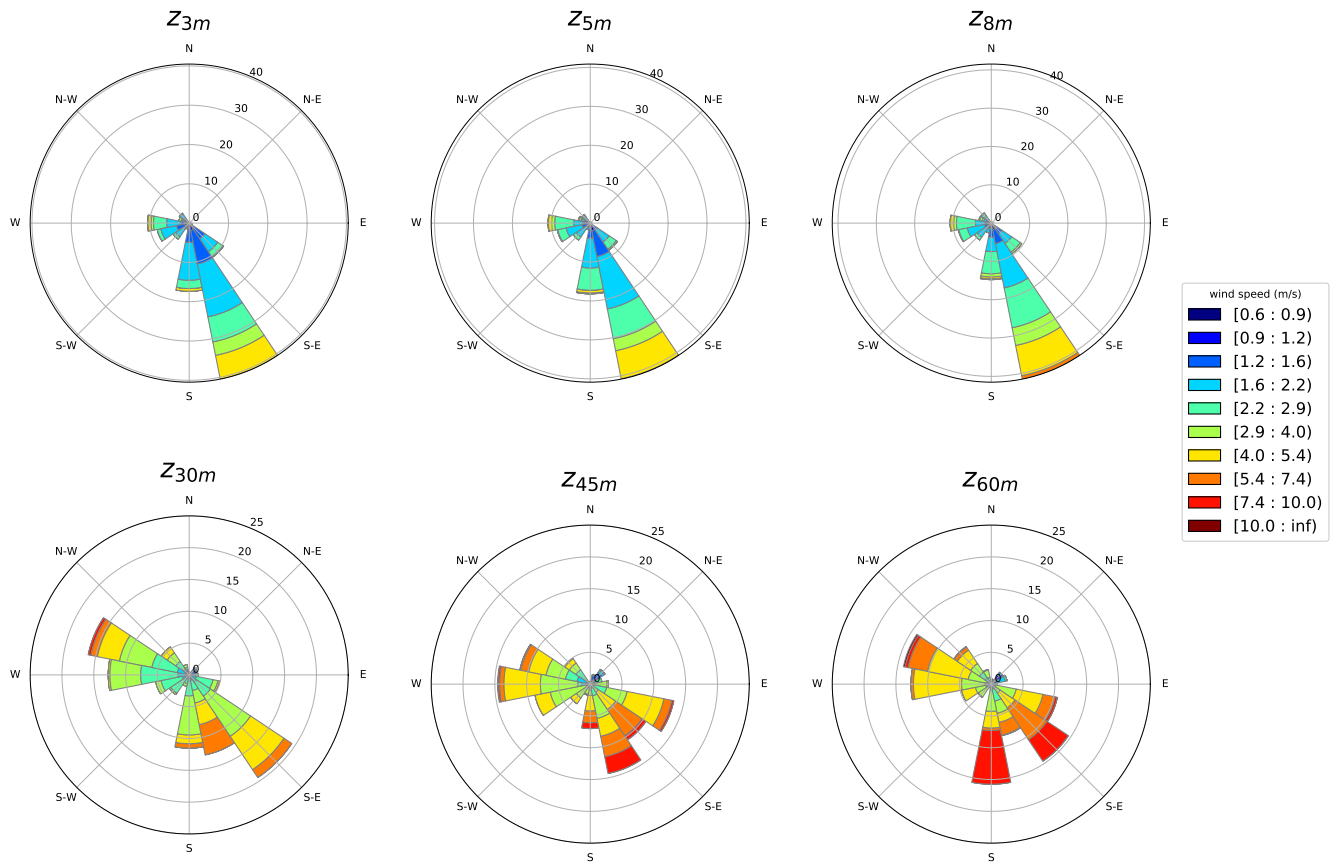
Figure 3. Night-time IOPs (nIOPs) wind roses for each level of the Skinflow mast (upper rows) and the Valimev tower (lower rows) during the BLLAST field campaign. Circles represent 10% frequency increments for the Skinflow mast levels, and 5% for the Valimev tower levels.

the uphill direction (Jimenez and Cuxart, 2014), with an average wind speed of $2 \, \mathrm{m \, s^{-1}}$. Later that day, the 2nd of July, at 1800 UTC, the wind turns to south – south-east, first at the lower levels, which correspond to drainage winds with lower velocities, and two hours later, at 2000 UTC, the wind veers towards south-east at all the levels increasing its velocity up to $5 \, \mathrm{m \, s^{-1}}$ associated with a mountain plain flow. The presence of a gully south to the Skinflow mast (Fig.2b) has a relevant effect on the

5 wind (Fig. 3) due to the frequent formation of a shallow drainage flow under very stable conditions (Nauta, 2013; Soler et al., 2002). The night flow for those stable nights has an intermittent nature since it is generated by drainage flows, mountain-plain and other mesoscale phenomena induced by the temperature gradients between the plains and the most northern mountain ranges of the Pyrenees located at the south of the site.

Fig. 3 also shows that the Valimev tower presents a remarkable fraction ($25 - 30 \, \%$ of all data), of winds from the west

10 and north-west, which can be closely connected to the fact that during the central part of the day preceding nIOPs, the wind is

from the north–north-west direction corresponding to the uphill direction, but turns to the south-east direction two hours after sunset, especially at the higher levels. As a consequence the north-west winds may prevail at high levels during nIOPs despite their anabatic origin.

Even though the main focus of this paper is the study of the HOST theory for the SBL, we also aim to analyse the behaviour of such theory for non nIOP conditions, and how the peculiarities of the Plateau de Lannemezan site affect its structure. Bearing this in mind we represent the wind rose for all the nigh-time set of data from the same levels of both towers (Fig. 4). One of the most relevant results for the Skinflow tower is the increasing frequency of winds coming from the westerly sector when all data is considered, unlike in nIOPs where westerly winds are almost negligible. The reason may be due to the fact that winds from the west and west–north-west direction, linked to larger-scale synoptic (Barneoud et al., 2010) flow, are very frequent in this part of Europe, with additional channelizing to westerlies due to the mountain range south of the site. The same result is observed for the Valimev tower, although winds from the south-east sector become slightly less dominant. For both data sets, south-east is clearly predominant for the Skinflow tower heights versus Valimev, this is because the first one has measurements at very low levels and therefore, for both datasets is able to measure small scale phenomena as SDF's which are generated by small scales as local slopes.

As we have seen throughout the flow characterization, the presence of shallow drainage flows, mountain plain flows, and the Aura valley jet favours the formation of LLJ with maximum winds at different heights. In addition, taking into account the results of previous work done by Nilsson et al. (2016) who through the analysis of the Skinflow mast derived wind profiles during 10 IOP nights, showed that all of them, except one, displayed reverse wind gradient or non-monotonic wind profile with wind direction from about 120 to 180 degrees. Therefore, we can argue that LLJs are a frequent phenomenon in BLLAST campaign. An exhaustive study about the relation between LLJs and turbulent regimes is out of the scope of this paper. However, followingSun et al. (2012) two possibilities can be considered, summarized in the following explanation:

a) The maximum wind of a LLJ is lower than the HOST threshold for its height above the ground, but the local shear below the LLJ is not negligible. Therefore moderate turbulence can be generated, diffusing downwards, especially when the vertical temperature gradient decreases with height. This situation leads to turbulence regime 3.

b) The maximum wind of a LLJ is greater than the HOST threshold for its height above the ground. In that case, regime 2 occurs.

By this way, in addition to other processes, the occurrence of the different regimes can be linked to the presence of LLJs.

After having classified and illustrated the flow circulation from the dataset, we analyse the turbulence regimes from two different perspectives: using only nIOPS data (Sect. 4) and using the whole BLLAST dataset (Sect. 5).

4 Turbulence regimes analysis: nIOPs

In this section we investigate the turbulence regimes using the data obtained from the so-called nIOPs in order to study the generality of the HOST pattern (Sun et al., 2012). We explore the dependence of the night-time turbulence intensity, V_{TKE},
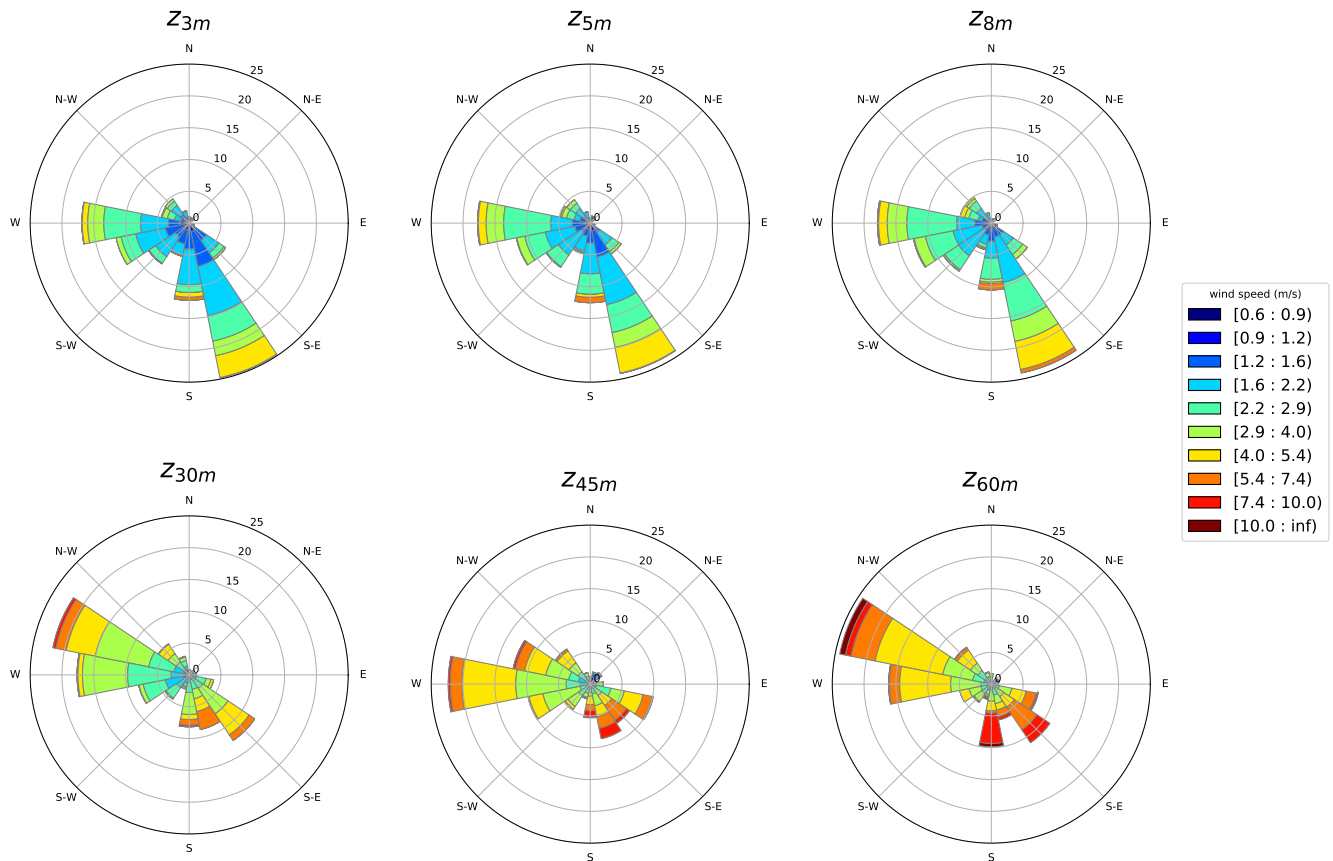
Figure 4. Night-time whole dataset wind roses for each level of the Skinflow mast (upper row) and the Valimev tower (lower row) during the BLLAST field campaign. Circles represent 5% frequency increments.

with the horizontal wind speed V for each of the observational levels. We also analyse the $V_{TKE}\ vs\ V$ relationship dependence on the thermal stratification through bulk virtual potential temperature differences between the Skinflow mast levels.

Fig. 5a shows the relationship between V_{TKE} and V, where the wind speed threshold is marked for every level (see triangles in Fig. 5a). The turbulence intensity relationships with V for the nIOPs have a similar hockey stick shape as the one obtained by Sun et al. (2012, 2016) using data from CASES-99. As described schematically in Fig. 1, Fig. 5a shows that for a given height, below a wind speed threshold, V_T, the turbulence intensity does not depend on the wind speed with no actual increase of V_{TKE} (regime 1). On the contrary, above a given V_T, V_{TKE} increases much more strongly than for lower wind speeds (regime 2). Table 3 shows the values of the wind speed thresholds obtained for the BLLAST field campaign during nIOPs. As observed by Sun et al. (2012) and Bonin et al. (2015), the wind speed threshold, V_T, (Table 3) also increases logarithmically with height in the BLLAST site during the nIOPs; the r^2 correlation between the logarithmic height and the wind speed is

around 0.92. The threshold value marks a change in the slope of the turbulence intensity relationship. Therefore, we consider that the regime changes to regime 2, when the slope has increased at least by two times the value of the slope of regime 1. The higher the layer, i.e. the deeper the stratus below z, the greater the value of V required for the layer to become neutral. Therefore, the V_T increases with height because larger shear production is needed to compensate for the inhibiting effect that near-surface stable stratification has on TKE. The V_T values for nIOPs in BLLAST are lower than those obtained by Sun et al. (2012) for CASES-99 and the bulk shear (V_T/z) is weaker as well (Fig. 5b). This can be explained by the effect of a larger roughness length in the BLLAST site, associated with the mountainous terrain south of the site. The greater the roughness length, the smaller the V_T, which means that weaker wind is necessary to achieve regime 2, as also seen by Mahrt et al. (2013).

It is also noticeable that the slope for the regime 2 for all the levels is quite similar, which indicates that, as expected, once the layer is neutral, the relationship between the turbulence intensity and the wind speed tends to be independent of the layer depth. Although the three turbulent regimes of the HOST pattern are visible at all levels, at the highest level, z_{60m}, the regime 2 does not seem to behave as expected for the greatest values of the wind speed, showing a decrease in the turbulence intensity as the V increases. This is due to the small amount of data for these wind speed bins, therefore no statistical conclusion can be drawn from it.

Table 3. Wind speed thresholds V_T for the Skinflow mast and Valimev tower levels for the BLLAST field campaign.

	z_{3m}	z_{5m}	z_{8m}	z_{30m}	z_{45m}	z_{60m}
V_T (m s^{-1})	1.3	1.7	2.1	3.7	6.1	6.9

The relationships of σ_V and σ_W with V (not shown) also present the HOST dependence seen for V_{TKE}. However, the turbulence values are generally smaller for σ_W with a smaller increase of the vertical variance with increasing V in regime 2 due to the ground impingement as found in Sun et al. (2012).

As turbulent mixing is influenced by the vertical temperature gradients, we now consider the effect of stratification on the turbulence relationship. We only proceed for the Skinflow mast because the separation of the measurements levels in the Valimev tower are too deep to calculate the stratification based on the bulk potential temperature difference, $\Delta \bar{\theta}_v$ (Sun et al., 2016). Herein $\Delta \bar{\theta}_v$ is defined as $\Delta \bar{\theta}_v = \bar{\theta}_v(z) - \bar{\theta}_{v_{z_0}}$, where $\bar{\theta}_{v_{z_0}}$ is the virtual potential temperature of reference at z_{2m}, and $\bar{\theta}_v(z)$ the virtual potential temperature at each height z. An alternative approach to calculate the stratification conditions could be to use the thermal gradient instead. However, throughout the paper we have considered the bulk potential temperature difference method described in Sun et al. (2016), which also provides good results and allows for a more consistent comparison within the Hockey-Stick theory framework.

In Fig. 6 we observe that for wind speeds greater than the threshold, $V > V_T$, the shear is strong enough to generate eddies with scale z, leading to a boundary layer neutrally stratified with a potential vertical temperature difference close to zero (green line). At all levels (Fig. 6 a, b, c) for wind speeds below the threshold, the stratification of the night-time boundary layer becomes stable, so there is a shallow mixing layer with a depth determined by $\delta z < z$ (Sun et al., 2012). Therefore turbulent eddies do not reach the surface and cold air is accumulated near the surface, resulting in layers with values of $\Delta \bar{\theta}_v > 0.5$ K.
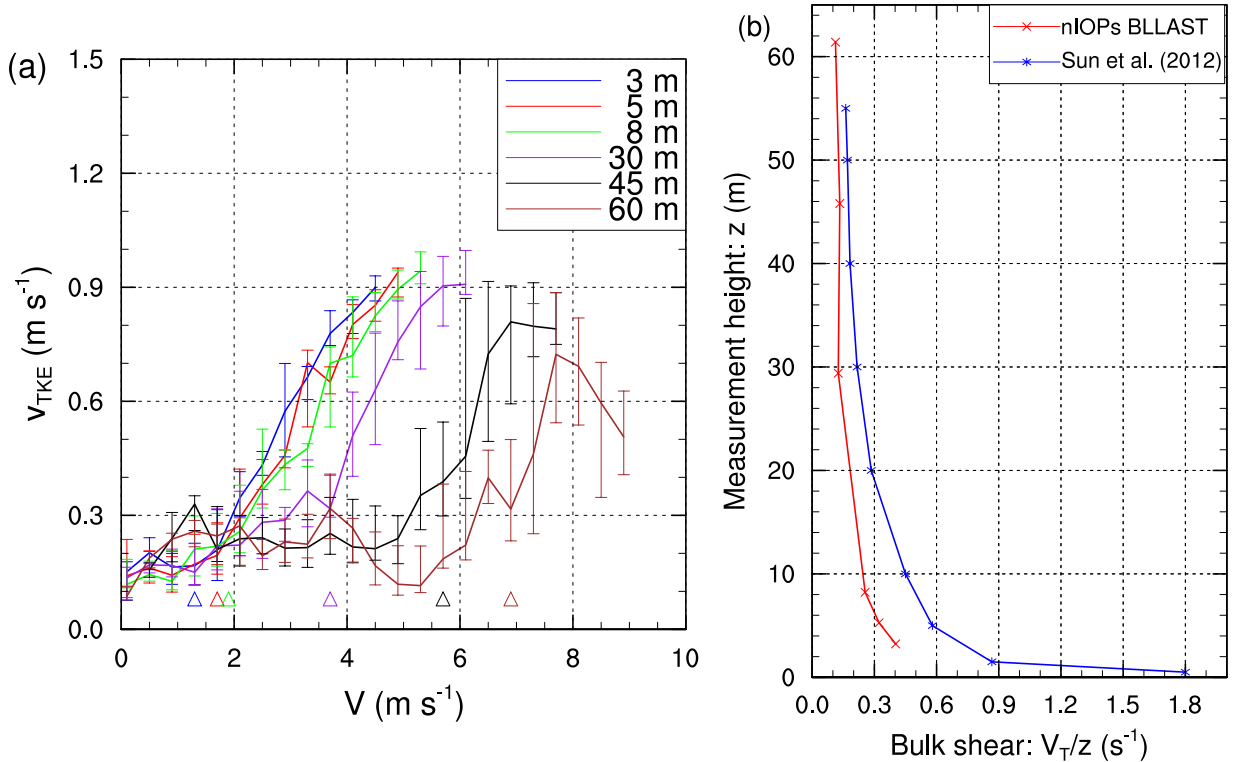
Figure 5. (a) Relationship between the bin-averaged turbulence intensity V_{TKE} and the wind speed V for the nIOPs of the BLLAST campaign. The lines join the median value of each V bin (0.4 m s^{-1} bins) for each level of measurement. The vertical lines of each bin mark the first and third quartiles with lower and upper end, respectively. The wind speed threshold V_T is marked with a coloured triangle for each coloured level. (b) Bulk shear variation with height obtained with BLLAST nIOPs data (red line) compared with CASES99 data reported by Sun et al. 2012 (blue line).

However, in Fig. 6 we observe situations that deviate from those described above. For example, in regime 1, for very stable situations ($\Delta \bar{\theta}_v > 0.5$ K), intermittent turbulence between regimes 1 and 2, and between regimes 1 and 3, can occur. Note that these transitions increase the turbulence, giving rise to temperature variations and mixing that would result in a near neutral or even unstable regime (see green and red lines in Fig. 6).

5   For $V > V_T$ the turbulent mixing processes tend to decrease the variability of $\Delta \bar{\theta}_v$ (Sun et al., 2016) and the stratification becomes near neutral. As it is expected, for $V < V_T$, the magnitude of the turbulence intensity, V_{TKE}, increases with decreasing values of $\Delta \bar{\theta}_v$, as the relevance of TPE decreases with instability (Zilitinkevich et al., 2007; Sun et al., 2016). Another important point to consider is the thickness of the layer, as $\Delta \bar{\theta}_v$ represents a vertically integrated virtual potential temperature difference, thus it will increase when the height of the level increases (Fig. 6 a, b, c). Therefore, due to the proximity between the z_{3m} and

10   z_{2m} levels most of the points fall into the stable-neutral stratification $0 \text{ K} < \Delta \bar{\theta}_v < 0.5$ K, which explains the predominance of
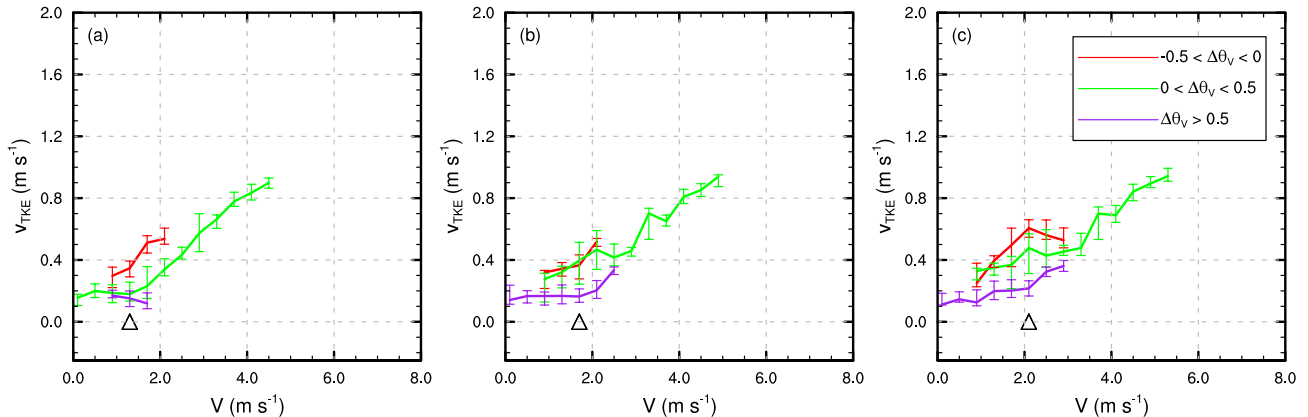
Figure 6. Relationship between the bin-averaged turbulence strength V_{TKE} and the wind speed V during the BLLAST campaign nIOPs as a function of potential temperature difference intervals, defined as, $\Delta\bar{\theta}_v = \bar{\theta}_v(z) - \bar{\theta}_{v_{z_0}}$, where $\bar{\theta}_{v_{z_0}}$ is the virtual potential temperature of reference at 2 m a.g.l., and $\bar{\theta}_v(z)$ the virtual potential temperature at each height z: (a) z_{3m}, (b) z_{5m}, and (c) z_{8m}. The wind speed threshold V_T is marked with a black triangle for each height (a) z_{3m}, (b) z_{5m}, and (c) z_{8m}.

the green line in Fig. 6a. For the z_{5m} and z_{8m} levels the amount of bins with larger values of $\Delta\bar{\theta}_v$ increases, as a consequence of being further up from the reference level.

5 Turbulence regimes analysis: whole BLLAST dataset

Herein we aim to explore how well the HOST behaves when we use all the night-time dataset from the BLLAST field campaign
5 without any restriction. To achieve this objective, we have done an analysis similar to the one followed in Sect. 4; we first analysed the turbulence relationship, then perform a deeper analysis using box plots for each measurement level, and finally examined turbulence relationships with the thermal stratification. Therefore, the first step is to analyse the differences between all the night-time data wind roses (Fig. 4) and those corresponding to nIOPs (Fig. 3). As we have seen in Sect. 3 the most remarkable feature is the high frequency of the western flows when the whole nocturnal dataset is considered. Taking into
10 account that many storms and frontal systems were from this direction (Barneoud et al., 2010), the analysis is done splitting the data between two sets of wind directions: the first group includes winds coming from directions ranging from $235°$ to $45°$, referred as NW's, including southwest to west, northwest, north and northeast directions; the second group includes the remaining directions, from $45°$ to $235°$ referred as SE's, including northeast to east, southeast, south and southwest directions, which are mostly due to the local topographic effects (Sect. 3).

13

5.1 Turbulence relationships

As in Sect. 4, we analyse the turbulence intensity relationships, but herein we focus on the whole night-time dataset without differentiating the fair weather nights to the non-fair weather nights. The analysis is done splitting the data into two main directions, flows coming from the NW's and the SE's directions (Fig. 7). For the NW's winds the relationship between the V_{TKE} with V is linear, so the HOST pattern cannot be appreciated (Fig. 7a). Contrary to this, for the SE's directions the V_{TKE} vs V does resemble to a hockey stick and we can distinguish a V_T for each height (Fig. 7b), which is similar to those found for the nIOPs but not equal, as the dataset herein includes all the night-time data. In fact, most of the SE's situations correspond to nIOPs (between a 63% and a 70% of them), so the hockey shape reproduced in Fig. 7b is very similar to that shown in Fig. 5. Indeed, this plot corresponds mostly to fair weather nights when stably stratified and near-neutral stratifications occurred and both regimes (regimes 1 and 2) could be distinguished. In contrast, situations corresponding to NW's are tied to frontal systems, cloud skies or cyclonic situations, which substantially modify the boundary layer ideal structure. Specifically, in these situations the surface may not have been warmed much during the day so nocturnal cooling effects were much more limited, then, the low-wind speed region of the HOST pattern is rarely reached and therefore regime 1 is not well illustrated in the V_{TKE} vs V relationship. For the NW's wind directions, the turbulence seems to be mainly driven by bulk shear, and the HOST turbulence intensity relationship may not be valid in those cases.

5.2 Box plots analysis

In order to further understand the turbulence behaviour, we illustrate the relationship between V_{TKE} and V using the box plots for each of the measured levels and wind speed bins as described in Sect. 2. To ensure representativeness of the box plots a minimum of six measurements for each bin is required. The method is a simple form to represent several simple statistics, such as the minimum and the maximum, the lower and upper quartiles and the median in a visual display. The amplitude of the box, i.e. the IQR, depends on the dispersion of the points within the bin, if V_{TKE} varies considerably for a given value of V, then the box will be larger. The whiskers length is proportional to the dispersion of V_{TKE}.

As can be seen in Fig. 8, Fig. 9 and Fig. A1 the V_{TKE} data distribution for each bin is not Gaussian and the upper whiskers are generally longer than the lower ones. This skewness is due to the non-existence of negative values and the fact that the turbulence intensity can be enhanced due to the presence of coherent structures, typical in regime 1 and transitioning to regime 3, i.e. for $V < V_{TKE}$. The quantity of outliers indicates the presence of turbulent events leading to an increase in the turbulent intensity which differs greatly from the value expected for a given range of V. This situation corresponds to regime 3 characterised by intermittent turbulence phenomena, which is typical for clear and calm nights.

The number of outliers within regime 3 is higher for wind speeds below the threshold, since the variability of the turbulence is higher. Instead, the strong wind associated with neutral stratification tends to suppress the occurrence of regime 3. It can be noted that for wind speeds closer to the threshold the scatter increases (Figs. 8d, 8e, 8f, 9d, 9e, 9f), which is due to the bin-averaged technique and the fact that around this velocity the turbulence intensity increases more quickly. The increase in scattering is observed in the IQR values, i.e. the larger length of the boxes, and in the greater amount of outliers.
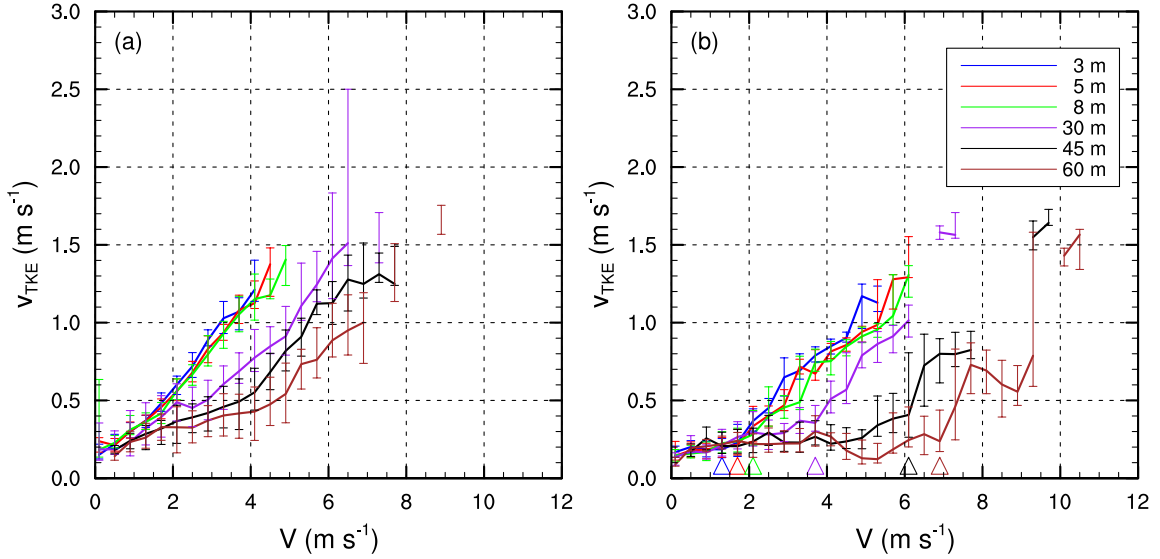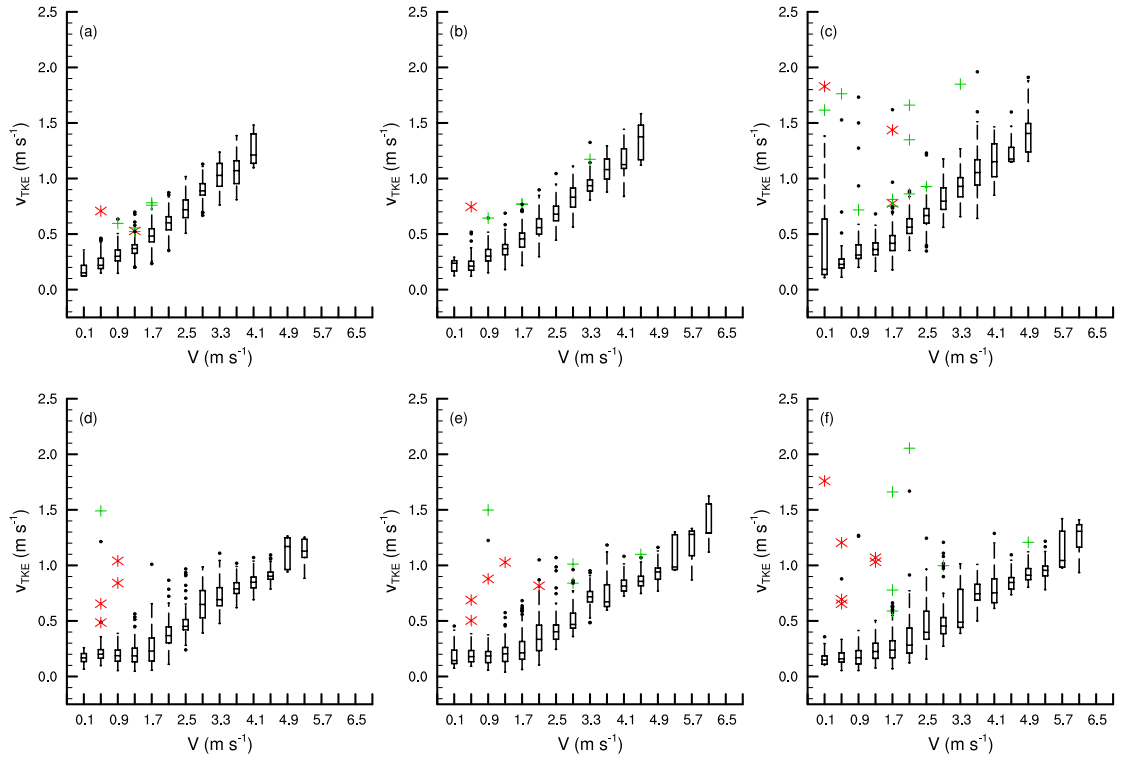
Figure 7. Relationships between the bin-averaged turbulence strength V_{TKE} and the wind speed V for the whole BLLAST field campaign for the main considered directions: (a) wind coming from $225°$ to $45°$ (included), named NW's, and (b) winds coming from $45°$ to $225°$ (included), named SE's. Each line represents the median within each 0.4 m s^{-1} V bin. The vertical lines represent the deviation for each V bin with the low limit corresponding to Q1 and the upper limit to Q3. The threshold wind speed V_T is marked with a triangle with the heights colours in (b).

We further examine the turbulence relationships separately for lower (Skinflow mast) and higher levels (Valimev tower). Thereafter we apply two conditions to distinguish the reason why the turbulence intensity is higher than expected. These points are outliers which have a very high V_{TKE} value, due to a quick change of the horizontal wind speed, ~ 1 m s^{-1}, between consecutive measurements (green crosses in Figs. 8 and 9) or to a shift in the wind direction of more than $\sim 75°$ between consecutive measurements (red asterisks in Figs. 8 and 9). These points represent enhanced turbulence intensity for a certain period, temporal average of 5 minutes, due to either wind speed shear or directional shear (Mahrt et al., 2013). Black dots are outliers not attributed to any of these shears, typical of regime 3, associated with top-down turbulent events.

In the following subsections we discuss the box plots for the Skinflow mast levels that are represented in Fig. 8 and the box plots for the Valimev tower levels in Fig. 9.

5.2.1 Skinflow mast levels

As seen in subsection 5.1, it is not expected that the relationship between V_{TKE} and V for the NW's directions will behave as the HOST predicts (Fig. 7), therefore, for these directions, a similar behaviour is seen for z_{3m} (Fig. 8a), z_{5m} (Fig. 8b) and z_{8m} (Fig. 8c) levels, where the turbulence strength increases near-linearly with V, and the first regime is not present. The whisker

Figure 8. Box plots of the relationship between the bin-averaged turbulence strength V_{TKE} and the wind speed V for the Skinflow night-time dataset for the whole BLLAST field campaign. The maximum whisker length is proportional to 1.5 times the third and first quartile difference, or inter-quartile range ($1.5 \cdot IQR$). The top row panels correspond to the NW's direction range for (a) NW's at z_{3m}, (b) NW's at z_{5m}, and (c) NW's at z_{8m} and the bottom row corresponds to the SE's directions, (d) SE's at z_{3m}, (e) SE's at z_{5m} and (f) SE's at z_{8m}. The outliers represent a turbulence enhancement due to a quick variation of the wind speed (greater than $1\,\mathrm{m\,s^{-1}}$) (green crosses), due to a sharp change in the wind direction (greater than $75°$) (red asterisks) or due to any other factor (black dots).

length is small except for lower and higher wind speeds at z_{8m}, hence the dispersion is low and most of the points are close to the median, so that the resulting relationship is fairly linear.

For the thermally driven flows the HOST pattern is clearly identified following both the whiskers and the median values of Fig. 8 d, e, f. There is also a large amount of enhanced turbulence points at all levels triggered mostly by wind speed and

5 directional shear. In addition, for regime 1, there is a large amount of black outliers close to the whiskers that can be related to regime 3, as top-down turbulent events associated with orographic effects are expected to occur from this direction. The IQR range tends to be small except for higher wind speeds, and the whiskers tend to be relatively close to the median. However, for wind speeds close to V_T the boxes and whiskers are longer, as the corresponding bin-averaged velocity includes turbulence intensities corresponding to the two different turbulence regimes, 1 and 2, with the later having greater V_{TKE} than the former.

When comparing the SE's box plots (Figs. 8d, 8e, 8f) with the nIOP box plots (Figs. A1a, A1b, A1c in the Appendix), the amount of outliers and the whisker length is considerably greater than for the nIOP situations. This large amount of outliers present in the SE's directions (Fig. 8d, 8e, 8f) is a remarkable difference from what was observed in Sun et al. (2012) and in the nIOPs box plot analysis (Fig. A1), where little dispersion was found for each V bin. This increase in the dispersion of the turbulence intensity values for a fixed V may be associated with the topography influence and specially with the weather conditions (synoptic scale), revealing an increase in the amount of non-stationary flows. While CASES-99 was located in a nearly flat terrain, BLLAST is a highly topographically influenced area, where, in addition, the presence of storms and low pressure systems affecting the region is common.

5.2.2 Valimev tower levels

For the Valimev tower we have made the same study as before, taking also into account the same main wind directions, NW's and SE's. One of the main results is related to both the IQR range and the whiskers length, for NW's and SE's, they both increase with the height of the measurement, indicating a wide variety of turbulence intensity cases (Fig. 9).

Similarly as in the Skinflow levels, the HOST pattern for the NW's directions cannot be appreciated, whilst for the SE's the turbulence intensity does follow the HOST pattern. For regime 1 in SE's (Fig. 9 d, e, f), even though the boxes are small, there is a great number of outliers, many of them very close to the whiskers which would correspond to regime 3. Turbulence enhancement due to wind speed shear dominates over wind directional shear at these levels. Many other outliers (black dots) close to the whiskers in regime 1 are identified as top-down turbulent events (e.g. Kelvin- Helmholtz instabilities, gravity waves or other intermittent turbulence events).

Similar to what was observed for the Skinflow mast levels, the comparison between the SE's box plots (Figs. 9d, 9e, 9f) and the nIOPs box plots (Figs. A1d, A1e, A1f in the Appendix), Valimev tower levels show a greater amount of outliers and a larger whisker length for the SE's box plots, which may be also linked to the topography influence and to the meteorological synoptic conditions.

Overall, for high wind speeds due to the lack of data, some box plots are not available, however the regime 2 pattern can be observed. The wind speed bins with values close to the V_T show greater dispersion (Fig. 8, Fig. 8 and Fig. A1) than the rest, indicating the inherent uncertainty in determining the observed V_T value.

5.3 Turbulence regimes and thermal stratification

To further understand the HOST pattern, as previously done in Sect. 4 for the nIOPs, we explore the effect of stratification on the turbulence relationship for the whole BLLAST dataset. We also separate the data depending on the two wind directions considered, NW's (Fig. 10a) and SE's (Fig. 10b). We only use data from the Skinflow mast, and because the results for the different levels, z_{3m}, z_{5m}, z_{8m} are very similar, we only do the analysis and the discussion for the z_{5m} level.

For the NW's flows (Fig. 10a), turbulent mixing leads to a neutral stratification (red and green lines) and also to unstable stratification (turquoise lines), indicating thermal instability in the flow. Stable stratification (purple line) only appears associated with very low velocities and with relatively large V_{TKE} values. Therefore, the linear turbulence relationship is independent
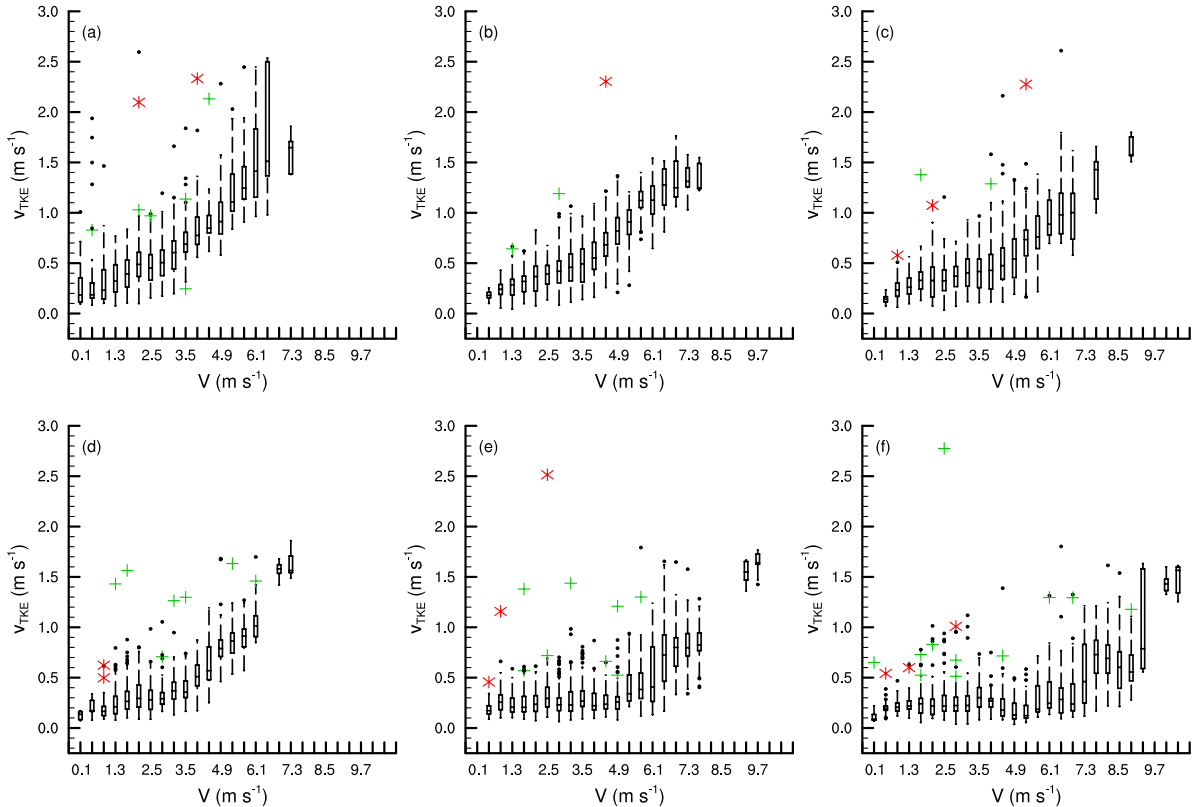
Figure 9. As Fig. 8 but for the Valimev dataset for the whole BLLAST field campaign. Top row panels correspond to the NW's direction range for (a) NW's at z_{30m}, (b) NW's at z_{45m}, and (c) NW's at z_{60m} and the bottom row corresponds to the SE's directions, (d) SE's at z_{30m}, (e) SE's at z_{45m} and (f) SE's at z_{60m}.

of the temperature gradients. Turbulence is driven by bulk shear, therefore the flow incoming from this direction is such that even for lower wind speeds it carries turbulence, i.e. large eddies, that produce similar V_{TKE} independently of the temperature gradient and of the stratification of the nocturnal ABL.

For the thermally driven flows (Fig. 10b) the behaviour of the turbulence intensity versus the wind speed depending on $\Delta\bar{\theta}_v$
5   is analogous to that found for the nIOPs (Sect. 4). Regime 1 is mostly associated with strong positive temperature gradients (purple lines) while near-neutral (green line) and unstable (red line) stratification is characteristic of regime 2 and 3. Indeed, the characteristic events of regime 3, can overturn the typical nocturnal positive temperature gradients.
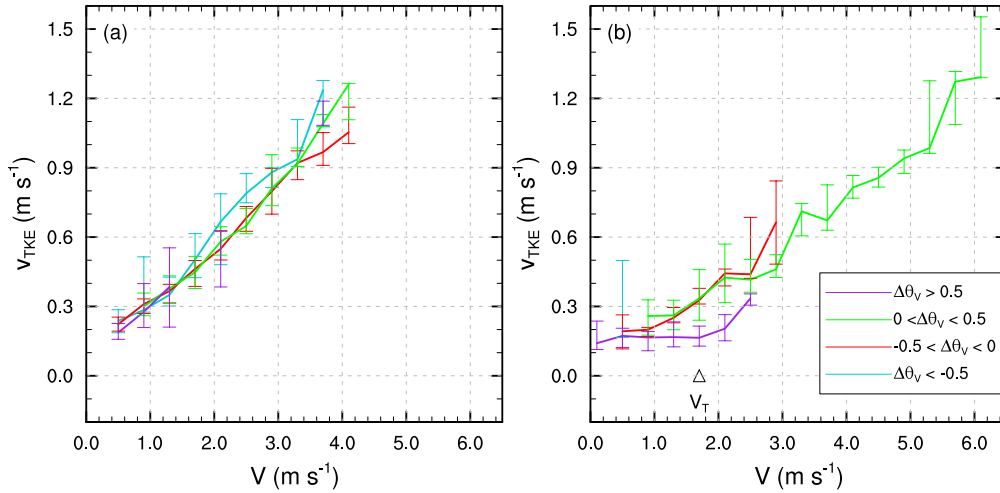
Figure 10. Relationship between the bin-averaged turbulence strength V_{TKE} and the wind speed V during the BLLAST campaign nIOPs as a function of potential temperature difference intervals, defined as, $\Delta\bar{\theta}_v = \bar{\theta}_v(z) - \bar{\theta}_{v_{z_0}}$, where $\bar{\theta}_{v_{z_0}}$ is the virtual potential temperature of reference at 2 m a.g.l., and $\bar{\theta}_v(z)$ the virtual potential temperature at the height of z_{5m} for: (a) NW's direction range and (b) SE's direction range. The wind speed threshold V_T for z_{5m} is marked with a black triangle in (b).

6 Transition between regimes and turbulence intermittency

Associated with the transition among the three turbulence regimes, Sun et al. (2012) defined three turbulent intermittency categories: A, B and C (Fig. 1). Category A corresponds to the transition between regime 1 and regime 2, and vice versa, the wind speed oscillates between both regimes generating intermittent turbulence. Category B corresponds to the enhancement of
5 turbulence within the regime 1 caused by atmospheric disturbances as internal gravity wave, density currents, and low-level jets (LLJs), that increases local turbulence and may reduce the local stability, even inducing some intermittency. Category C refers to top-down turbulent events or upside-down boundary layers that enhance downward turbulence into a stable environment, generating regime 3. Since the HOST theory and the related intermittency categories were defined for the SBL, here we only consider the nIOPs and we illustrate the previous categories selecting appropriate examples.

6.1 Turbulence intermittency: Categories A & B

10 During the BLLAST field campaign the occurrence of winds influenced by the complex orography at the south of the site was common (Fig. 3). At this site, they are usually generated after the near calm situation of the evening transition, first as shallow drainage flows, and then interrupted by the arrival of a larger and deeper mountain-plain flow with greater values of V(Román-Cascón et al., 2015; Jiménez et al., 2019). The transition between them can cause wind speed oscillations between regime 1
15 and 2, and shallow wind oscillations within regime 1 leading to turbulence intermittency of category A and B respectively.

During the BLLAST field campaign both type of transitions are detected, either by the Valimev tower or by both the Valimev and the Skinflow levels. In almost every nIOP one of the different ways of achieving this category of turbulence intermittency is observed. For this study we select the period between 1900 UTC and 2200 UTC during the night of the 2nd of July of 2011 (nIOP09) (Román-Cascón et al., 2015), as it represents better the intermittency of both of these categories (Fig. 11). The

5 categories can also be found during other nIOPs. Category A can be found in all the nIOP cases but nIOP10. Category B is not so frequent, occurring for short periods during the nIOPs 01, 02, 03, 04, 05, 07, 09.

The 2nd of July of 2011 (IOP10) was characterised by an anticyclonic situation over the south of France, leading to weak surface gradients and to near calm conditions close to the surface at the evening time. Thus, at 1900 UTC the wind speed values are around 0.5 m s^{-1}(Fig. 11a). This situation is, according to Román-Cascón et al. (2015), the foremost scenario for

10 "the appearance of SDFs with a marked SSE-SE component, where stronger winds were encountered at lower levels with maxima close to the surface (around 2-3 m above ground) and the wind intensity decreasing with height above the maximum". This is the picture of a slight SDF flowing through the nearby gully (Nauta, 2013; Román-Cascón et al., 2015) measured by the Skinflow mast and the Valimev towers, although in Fig. 11 only the z_{30m} level of Valimev tower is shown, for better clarity. The arrival of this SDF promotes the establishment of a surface temperature inversion (Fig. 11b), with a larger decrease in

15 temperature at the lowest levels. The SDF stage ends around 2025UTC with the arrival of a stronger and deeper wind (Fig. 11a) from the southeast, and the MPF stage starts. This increase in wind is more noticeable at high levels, leading to the breaking of the SDF and the potential virtual potential temperature homogenisation (Fig.11b).

As Román-Cascón et al. (2015) showed, two different gravity wave events occurred during the SDF stage and the arrival of the MPF. Both events are examples of turbulence intermittency categories. The first one corresponds to a wave of almost four

20 cycles with a 20-25 min period between 19:00 and 2025 UTC approximately. This is an example of category B of turbulence intermittency, as the oscillations in wind speed occur for wind speeds below the threshold of each level (see the V$_T$ for each height marked with a coloured horizontal dashed line in Fig. 11a), within regime 1. The turbulence can be seen clearly for z_{2m}, z_{3m}, z_{5m} and z_{30m} (see category B ("Cat. B" arrow in Fig. 11a). Román-Cascón et al. (2015) states that the second event "is characterised by several wind speed oscillations of shorter periods with two notable cycles of greater amplitude from 2030 to

25 2130 UTC". The wind speed oscillates around the threshold, as an example of category A. There is a transition from regime 1 to 2 and viceversa at z_{3m}, z_{5m}, z_{8m} and z_{30m} (see category A "Cat.A" in Fig. 11a). In addition, when the wind speed is above the threshold, the virtual potential temperature vertical gradients are reduced (Fig. 11b), as it is expected in regime 2.

## 6.2 Turbulence intermittency: Category C

Category C turbulence intermittency refers to the transition between regimes 1 and 3 in the HOST model (Fig. 1). It is originated

30 in very stable boundary layers when the main source of turbulence is elevated, and is temporally detached from the surface but intermittently coupled to the surface generating bursts of downward turbulence (Blumen et al., 2001). The origin of this elevated turbulence can be related to the presence of Kelvin-Helmholtz instabilities, density currents, gravity waves, low level jets or any other meteorological phenomena that can induce turbulence intermittency (Mahrt, 2014; Udina et al., 2013; Ferreres et al., 2013; Soler et al., 2014)
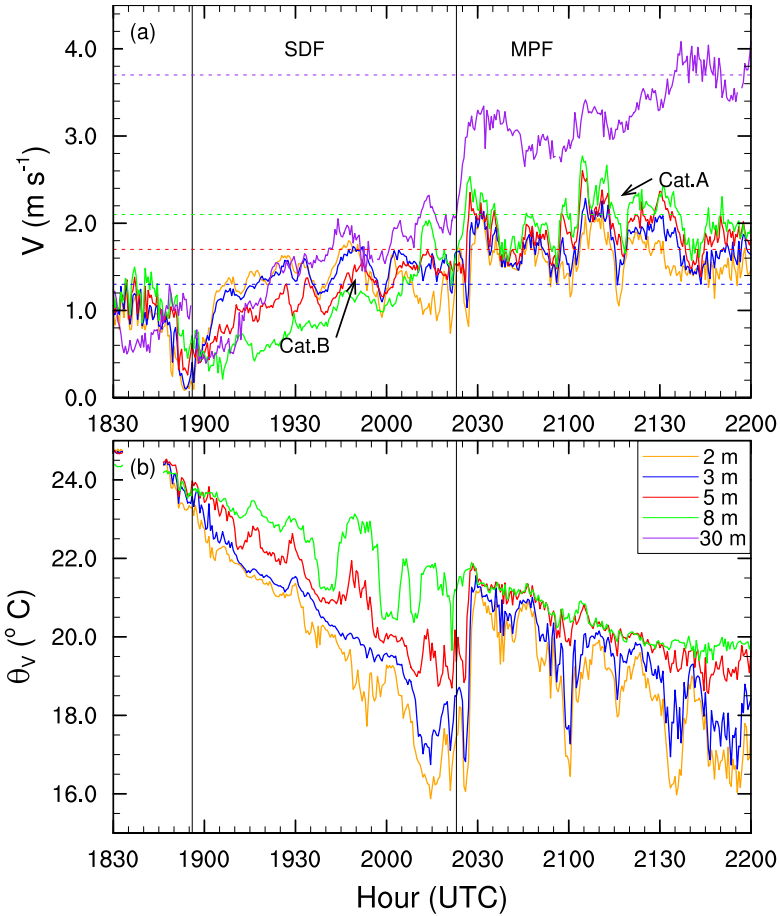
Figure 11. Time series of (a) horizontal wind speed and (b) virtual potential temperature for the 2 of July (nIOP09) during the BLLAST field experiment for z_{2m}, z_{3m}, z_{5m}, z_{8m} and z_{30m}. The shallow drainage flow (SDF) stage is indicated between 1855 and 2020 UTC, and a consecutive mountain-plain flow (MPF) stage thereafter. In the SDF stage there are oscillations within regime 1, which is category B, whereas in MPF stage there are transitions between regime 1 and regime 2. The potential temperature is not represented for z_{30m} because there are thermocouple measurements only for the Skinflow mast (z_{2m}-z_{8m}). The wind speed threshold for several levels are marked with the dashed line to better illustrate the transitions, whilst some transitions between regime 1 and regime 2 are marked with an arrow. The data shown herein is the 30 s temporal average from sonic anemometers with a frequency of 10 Hz.

Usually, category C turbulence intermittency is characterised by a decrease of V, an increase in the variability of w with height, and negative values of the skewness S (Blumen et al., 2001; Sun et al., 2012), meaning a downward transport of turbulence (Mahrt and Vickers, 2002).

In order to illustrate an example of category C turbulence intermittency, we select an event taking place between 0300 and
5 0400 UTC of 26 of June of 2011, nIOP05. From Fig. 12a we can observe a progressive wind speed decrease in the higher

21
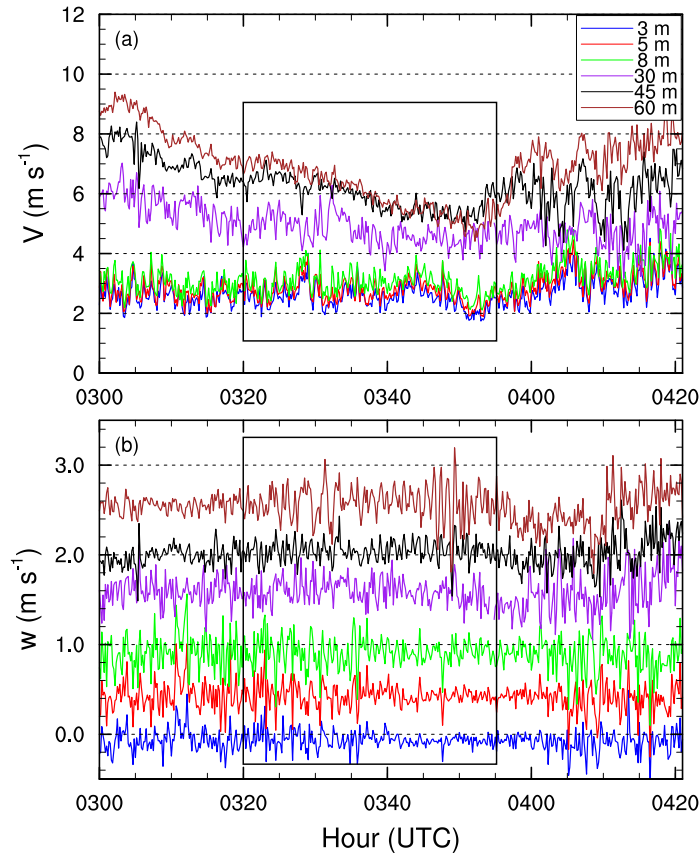
Figure 12. Times series of (a) horizontal wind speed V and (b) vertical wind speed, w (incremented $0.5\ \mathrm{m\ s^{-1}}$ for an easy comparison) for 26 June 2011 at z_{3m}, z_{5m}, z_{8m}, z_{30m}, z_{45m} and z_{60m}. The black rectangle marks the top-down event. The data shown herein is the 10 s temporal average from sonic anemometers with a frequency of 10 Hz.

levels of the Valimev tower between 0310 and 0350 UTC (see black rectangle in Fig. 12a), associated with an increase on the vertical wind speed variability at 60 m, which has the maximum between 0345 and 0355 UTC (Fig. 12b). This maximum increases with height and propagates downward to lower levels with time. This downward turbulence transport is also reflected in negative S values, shown in Fig. 13 for z_{8m} and z_{60m}. The period where the skewness is more negative agrees well with the period at which the larger oscillations of w take place (0350 UTC). All these characteristics could indicate a turbulence intermittency event corresponding to category C. The event exhibits occasional mixing and a downward transport of turbulence (Mahrt and Vickers, 2002), both suggesting a possible top-down turbulence event. It is relevant to note that this event is not strong enough to arrive to the lowest levels of the Skinflow mast.
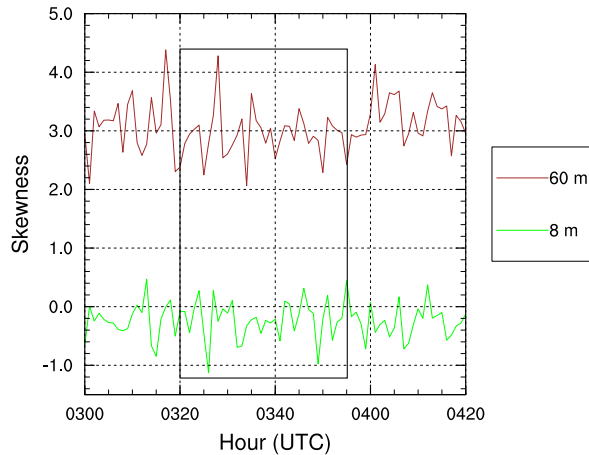
Figure 13. Time evolution of skewness of vertical wind component measured between 0300 and 0400 UTC on 26 of June during the BLLAST field experiment for the levels z_{3m} and z_{60m}. For the sake of clarity, the 60 m level skewness measurements are increased by 3 m s^{-1}. The black rectangle localises the top-down event. The data shown herein is the 1 min temporal average from sonic anemometers with a frequency of 10 Hz.

Category C turbulence intermittency does not occur as often as category A and category B, as the number of points within regime 3 in Figs. A1, 8, and 9 shows. These points could sometimes correspond to a top-down event, but not always, since the regime 3 can be achieved through accelerations and sharp wind direction shifts (Mahrt et al., 2013).

7 Conclusions

In this study we have analysed the HOST theory proposed by Sun et al. (2012) using the nocturnal data set of the BLLAST campaign, that took place at the "Plateau de Lannemezan", an area located north of the central French Pyrenees. The main objective has been to explore the influence of the orography and the weather conditions during the BLLAST campaign in the HOST pattern that was originally defined for a relatively flat area and for fair weather conditions, the predominant conditions of the CASES-99 field campaign. Here, the analysis has been done separating nights into two types: nocturnal IOPs (nIOPs) and the whole nocturnal dataset.

For the nIOPs of the BLLAST campaign the HOST theory is found to be valid and the turbulence relationships show the different turbulence regimes with a wind speed threshold for each height which locates the transition between the weak wind and weak turbulence intensity generated by local shear, regime 1, and the strong turbulence intensity generated by bulk shear, regime 2. This wind speed thresholds are lower than in Sun et al. (2012) so the bulk shear needed to achieve regime 2 is lower as well, due to the greater roughness length of the mountainous terrain linked with the incoming southern flow. Similar results were found by Mahrt et al. (2013) and Bonin et al. (2015) for other locations. These nights are characterised by clear skies

23

and intense radiative cooling where the predominant flow comes from the south-east quadrant corresponding to the arrival of shallow drainage flows to the lower levels and mountain plain flows later on. These flow circulations generated by the orography lead to turbulence enhancement and transitions between regimes, modifying the ideal HOST pattern.

Instead, when the turbulence relationship is analysed for the whole night dataset, results are significantly different, and they become wind direction dependent. The HOST pattern is observed for thermally driven flows, from wind directions between 45° and 235° (SE's) but it cannot be appreciated for winds coming for the other directions (NW's). For the NW's flows, the turbulence relationship is almost linear and independent of the vertical temperature gradients. Indeed, when considering the whole night-time dataset the frequency of winds coming from westerly and northerly directions increases representing the synoptic scale meteorological situations, in which the HOST pattern is erased mainly because the stable boundary layer cannot be developed.

To further investigate the turbulence relationship, we used box plots to provide additional information. Comparing the nIOPs and the SE's flows from the whole nocturnal dataset there are interesting differences: (i) the turbulence intensity tends to increase when we use the whole nocturnal SE's dataset; (ii) the number of outliers increases for the whole nocturnal SE's dataset, and therefore the number of turbulent events associated with transitions between regimes 1, 2 and 3. Several points falling in regime 3 are actually associated with sudden wind speed and wind directional shear transitions, reflecting the non-stationary nature of regime 3.

In addition, when HOST is achieved, near neutral stratification is tied to regime 2, where turbulence is driven by bulk shear. Instead, when $V < V_T$ stable stratification dominates, although negative potential temperature differences are present when intermittent turbulence events occur.

Finally, the different transitions between the HOST regimes related to turbulence intermittency (categories A, B and C) are illustrated for some nIOPs using appropriate examples. Results show that the presence of gravity waves associated with shallow drainage flows and mountain plain flows create intermittent turbulence that can lead to a transition between regime 1 and regime 2, an example of category A. Local shear can be generated by internal gravity waves of relatively small wind speed amplitude so that the wind speed is lower than the threshold value. As a result, there is an increase of turbulence within regime 1 (Sun et al., 2012), which is the category B turbulence transition. Mahrt (2010) found that with very weak winds and strong stratification (regime 1), turbulence can appear under the presence of gravity waves. These oscillations are typically originated within the shallow drainage flow. Category C may also appear when turbulence created by wind speed or directional shear is diffused downward, toward a stable environment.

Present and future work related to the knowledge of the flow circulation in BLLAST site would help to the full understanding of the results obtained herein. In addition, a deeper and longer-term study of the HOST theory in other locations considering mountain influenced sites and complex terrain areas would be desirable so that our outcomes could be generalised.

Appendix A: Box plot analysis during nIOPs

This appendix is devoted to complement Sect. 3 showing the relationship between the V_{TKE} and V for the nIOP cases using box plot analysis (Fig. A1). It can be seen clearly how the results obtained herein display the same HOST theory as in Sun et al. (2012) for the CASES-99 field campaign.
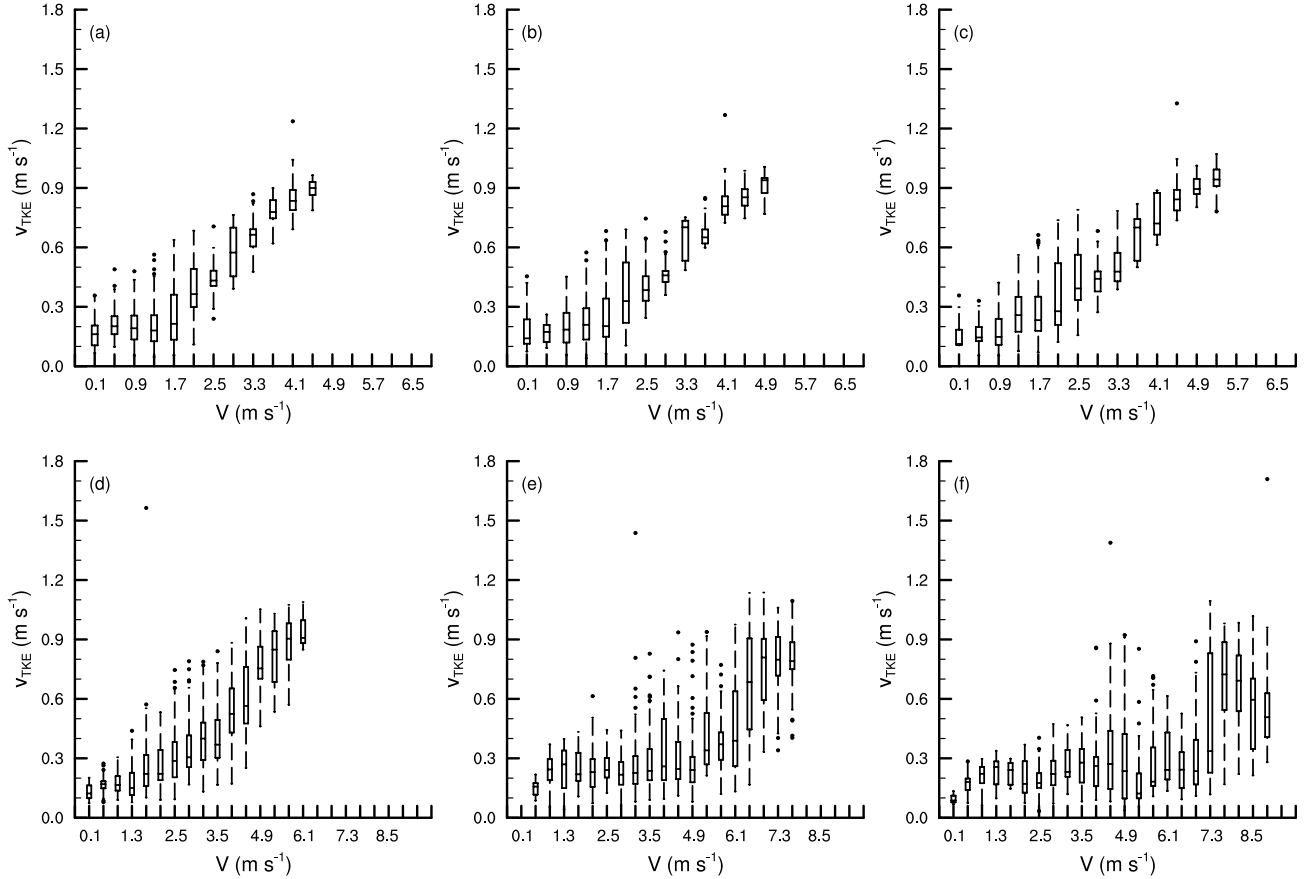
Figure A1. Box plots of the relationship between the bin-averaged turbulence strength V_{TKE} and the wind speed V for the nIOPs of the BLLAST field campaign. The maximum whisker length is proportional to 1.5 times the third and first quartile difference, or inter-quartile range ($1.5 \cdot IQR$). Data correspond to the Skinflow mast and to the Valimev tower at different heights, (a) z_{3m}, (b) z_{5m} and (c) z_{8m} Skinflow mast levels, and (d) z_{30m}, (e) z_{45m} and (f) z_{60m} Valimev tower levels.

helpful information on the HOST theory and ideas for improvement on the initial idea. Joan Bech, altogether with everyone provided help on the manuscript structure and general advice on turbulence. Maria Rosa Soler and Mireia Udina played a crucial part in the processes of crafting this manuscript from scratch with Jesús Yus-Díez, developing the data process, the analysis of the results, and summarizing and expressing it in this article.

References

Acevedo, O. C., Mahrt, L., Puhales, F. S., Costa, F. D., Medeiros, L. E., and Degrazia, G. A.: Contrasting structures between the decoupled and coupled states of the stable boundary layer, Quarterly Journal of the Royal Meteorological Society, 142, 693–702, 2016.

Andreae, M., Acevedo, O., Araújo, A., Artaxo, P., Barbosa, C., Barbosa, H., Brito, J., Carbone, S., Chi, X., Cintra, B., et al.: The amazon
5   tall tower observatory (ATTO) in the remote Amazon basin: overview of first results from ecosystem ecology, meteorology, trace gas, and aerosol measurements., Atmospheric Chemistry & Physics Discussions, 15, 2015.

Barneoud, P., Beck, S., Lafrique, P., and Lagnoux, B.: Climatologie sur le site instrumenté du Laboratoire d'Aérologie, 2010.

Blay-Carreras, E., Pardyjak, E., Pino, D., Alexander, D., Lohou, F., and Lothon, M.: Countergradient heat flux observations during the evening transition period, Atmospheric Chemistry and Physics, 14, 9077–9085, 2014.

10   Blumen, W. ., Banta, R., Burns, S., Fritts, D., Newson, R., Poulos, G., and Sun, J.: Turbulence statistics of a Kelvin-Helmholtz billow event observed in the night-time boundary layer during the Cooperative Atmosphere-Surface Exchange Study field program, Dynamic of Atmospheres and Oceans, 34, 189–204, 2001.

Bonin, T. A., Blumberg, W. G., Klein, P. M., and Chilson, P. B.: Thermodynamic and turbulence characteristics of the southern great plains nocturnal boundary layer under differing turbulent regimes, Boundary-layer meteorology, 157, 401–420, 2015.

15   Cuxart, J. and Jiménez, M.: Mixing processes in a nocturnal low-level jet: An LES study, Journal of the atmospheric sciences, 64, 1666–1679, 2007.

De Coster, O., Pietersen, H. P., Lohou, F., Hartogensis, O., and Moene, A.: BLLAST-uniform processing of Eddy-Covariance data, Internship Report Meteorology and Climatology, Wageningen University and Research Center, 990, 2011.

Ferreres, E., Soler, M., and Terradellas, E.: Analysis of turbulent exchange and coherent structures in the stable atmospheric boundary layer
20   based on tower observations, Dynamics of atmospheres and oceans, 64, 62–78, 2013.

Jimenez, M. and Cuxart, J.: A study on the nocturnal flows generated in the north side of the Pyrenees, Atmospheric Research, 145-146, 244–254, 2014.

Jiménez, M. A., Cuxart, J., and Martínez-Villagrasa, D.: Influence of a valley exit jet on the nocturnal atmospheric boundary layer at the foothills of the Pyrenees, Quarterly Journal of the Royal Meteorological Society, 145, 356–375, 2019.

25   Lin, J.-T. and Pao, Y.-H.: Wakes in stratified fluids, Annual Review of Fluid Mechanics, 11, 317–338, 1979.

Lothon, M., Lohou, F., Pino, D., Couvreux, F., Pardyjak, E., Reuder, J., Vilà-Guerau De Arellano, J., Durand, P., Hartogensis, O., Legain, D., et al.: The BLLAST field experiment: boundary-layer late afternoon and sunset turbulence, Atmospheric chemistry and physics, 14, 10 931–10 960, 2014.

Mahrt, L.: Stratified atmospheric boundary layers, Boundary-Layer Meteorology, 90, 375–396, 1999.

30   Mahrt, L.: Computing turbulent fluxes near the surface: Needed improvements, Agricultural and forest meteorology, 150, 501–509, 2010.

Mahrt, L.: Stably stratified atmospheric boundary layers, Annual review of fluid mechanics, 46, 23–45, 2014.

Mahrt, L.: Stably stratified flow in a shallow valley, Boundary-layer meteorology, 162, 1–20, 2017.

Mahrt, L. and Vickers, D.: Contrasting vertical structures of nocturnal boundary layers, Boundary-Layer Meteorology, 105, 351–363, 2002.

Mahrt, L., Thomas, C., Richardson, S., Seaman, N., Stauffer, D., and Zeeman, M.: Non-stationary generation of weak turbulence for very
35   stable and weak-wind conditions, Boundary-Layer Meteorology, 147, 179–199, 2013.

Nauta, L.: Shallow drainage flows over light sloping terrain during BLLAST 2011: Two case studies, Master's thesis, Meteorology and air quality group at the Wageningen University, supervised by Dr.Ir. Oscar Hartogensis, 2013.

Newsom, R. K. and Banta, R. M.: Shear-flow instability in the stable nocturnal boundary layer as observed by Doppler lidar during CASES-99, Journal of the atmospheric sciences, 60, 16–33, 2003.

Nilsson, E., Lohou, F., Lothon, M., Pardyjak, E., Mahrt, L., and Darbieu, C.: Turbulence kinetic energy budget during the afternoon transition–Part 1: Observed surface TKE budget and boundary layer description for 10 intensive observation period days, Atmospheric Chemistry and Physics, 16, 8849–8872, 2016.

Poulos, G. S., Blumen, W., Fritts, D. C., Lundquist, J. K., Sun, J., Burns, S. P., Nappo, C., Banta, R., Newsom, R., Cuxart, J., et al.: CASES-99: A comprehensive investigation of the stable nocturnal boundary layer, Bulletin of the American Meteorological Society, 83, 555–581, 2002.

Román-Cascón, C., Yagüe, C., Arrillaga, J., Lothon, M., Pardyjak, E., Lohou, F., Inclán, R., Sastre, M., Maqueda, G., Derrien, S., et al.: Comparing mountain breezes and their impacts on CO2 mixing ratios at three contrasting areas, Atmospheric Research, 221, 111–126, 2019.

Román-Cascón, C., Yagüe, C., Mahrt, L., Sastre, M., Steeneveld, G.-J., Pardyjack, E., van de Boer, A., and Hartogenesis, O.: Interactions among drainage flows, gravity waves and turbulence: a BLLAST case study, Atmospheric Chemistry and Physics, 14, 9031–9047, 2015.

Said, F., Derrien, S., Pique, E., Abadie, M., Meyerfeld, Y., Jarnot, C., Martin, J., Bezombes, Y., Lohou, F., Lothon, M., Rechal, R., and Bargain, E.: POCTEFA/FluxPyr and BLLAST Campistrous mast June 2011, http://bllast.sedoo.fr/database/source/displayDataCorps.php?pi=Fabienne.Lohou@aero.obs-mip.fr&rep=../data/FREE/Ground_Station/60_m_Tower/fiches_Meteorologicalparameters/, 2011a.

Said, F., Derrien, S., Pique, E., Abadie, M., Meyerfeld, Y., Jarnot, C., Martin, J., Bezombes, Y., Lohou, F., Lothon, M., Rechal, R., and Bargain, E.: POCTEFA/FluxPyr and BLLAST Campistrous mast July 2011, http://bllast.sedoo.fr/database/source/displayDataCorps.php?pi=Fabienne.Lohou@aero.obs-mip.fr&rep=../data/FREE/Ground_Station/60_m_Tower/fiches_Meteorologicalparameters/, 2011b.

Soler, M., Infante, C., Buenestado, P., and Mahrt, L.: Observations of nocturnal drainage flow in a shallow gully, Boundary-Layer Meteorology, 105, 253–273, 2002.

Soler, M., Udina, M., and Ferreres, E.: Observational and numerical simulation study of a sequence of eight atmospheric density currents in northern Spain, Boundary-layer meteorology, 153, 195–216, 2014.

Sun, J.: Vertical variations of mixing lengths under neutral and stable conditions during CASES-99, Journal of Applied Meteorology and Climatology, 50, 2030–2041, 2011.

Sun, J., Burns, S. P., Lenschow, D. H., Banta, R., Newsom, R., Coulter, R., Frasier, S., Ince, T., Nappo, C., Cuxart, J., et al.: Intermittent turbulence associated with a density current passage in the stable boundary layer, Boundary-Layer Meteorology, 105, 199–219, 2002.

Sun, J., Lenschow, D. H., Burns, S. P., Banta, R. M., Newsom, R. K., Coulter, R., Frasier, S., Ince, T., Nappo, C., Balsley, B. B., et al.: Atmospheric disturbances that generate intermittent turbulence in nocturnal boundary layers, Boundary-Layer Meteorol, 110, 255–279, 2004.

Sun, J., Mahrt, L., Banta, R., and Pichugina, Y. L.: Turbulence regimes and turbulence intermittency in the stable boundary layer during CASES99, Journal of the Atmospheric Sciences, pp. 338–351, 2012.

Sun, J., Lenschow, D. H., LeMone, M. A., and Mahrt, L.: The role of large-coherent-eddy transport in the atmospheric surface layer based on CASES-99 observations, Boundary-layer meteorology, 160, 83–111, 2016.

Terradellas, E., Soler, M., Ferreres, E., and Bravo, M.: Analysis of oscillations in the stable atmospheric boundary layer using wavelet methods, Boundary-layer meteorology, 114, 489–518, 2005.

Udina, M., Soler, M., Viana, S., and Yagüe, C.: Model simulation of gravity waves triggered by a density current, Quarterly Journal of the Royal Meteorological Society, 139, 701–714, 2013.

Udina, M., Sun, J., Kosović, B., and Soler, M. R.: Exploring vertical turbulence structure in neutrally and stably stratified flows using the weather research and forecasting–large-eddy simulation (WRF–LES) model, Boundary-layer meteorology, 161, 355–374, 2016.

Viana, S., Terradellas, E., and Yagüe, C.: Analysis of gravity waves generated at the top of a drainage flow, Journal of the Atmospheric Sciences, 67, 3949–3966, 2010.

Wyngaard, J. C.: Turbulence in the Atmosphere, Cambridge University Press, Cambridge, UK, 393 pp, 2010.

Zilitinkevich, S., Elperin, T., Kleeorin, N., and Rogachevskii, I.: Energy-and flux-budget (EFB) turbulence closure model for stably stratified flows. Part I: steady-state, homogeneous regimes, pp. 11–35, 2007.

5